CARBON 48 (2010) 1592–1597

available at www.sciencedirect.com

ScienceDirect

journal homepage: www.elsevier.com/locate/carbon

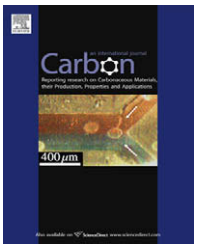

Quantifying ion-induced defects and Raman relaxation length in graphene

M.M. Lucchese [a], F. Stavale [a], E.H. Martins Ferreira [a], C. Vilani [a], M.V.O. Moutinho [b], Rodrigo B. Capaz [a,b], C.A. Achete [a,c], A. Jorio [a,d,*]

[a] Divisão de Metrologia de Materiais, Instituto Nacional de Metrologia, Normalização e Qualidade Industrial (INMETRO), Duque de Caxias, RJ 25250-020, Brazil

[b] Instituto de Física, Universidade Federal do Rio de Janeiro, Cx. Postal 68528, Rio de Janeiro, 21941-972 RJ, Brazil

[c] Programa de Engenharia Metalúrgica e de Materiais (PEMM), Univ. Federal do Rio de Janeiro, Cx. Postal 68505, Rio de Janeiro, 21945-970 RJ, Brazil

[d] Dept. de Física, Universidade Federal de Minas Gerais, Belo Horizonte, MG 30123-970, Brazil

ARTICLE INFO

Article history:
Received 16 October 2009
Accepted 24 December 2009
Available online 6 January 2010

ABSTRACT

Raman scattering is used to study disorder in graphene subjected to low energy (90 eV) Ar^+ ion bombardment. The evolution of the intensity ratio between the G band (1585 cm^{-1}) and the disorder-induced D band (1345 cm^{-1}) with ion dose is determined, providing a spectroscopy-based method to quantify the density of defects in graphene. This evolution can be fitted by a phenomenological model, which is in conceptual agreement with a well-established amorphization trajectory for graphitic materials. Our results show that the broadly used Tuinstra-Koenig relation should be limited to the measure of crystallite sizes, and allows extraction of the Raman relaxation length for the disorder-induced Raman scattering process.

1. Introduction

In carbon materials, mechanical properties can be improved and the synthesis of new phases can be induced by introducing controlled amounts of lattice damage [1,2]. Raman spectroscopy has been largely used to identify disorder in the sp^2-network of different carbon structures [3–8]. The Raman signature for disorder is the observation of the so-called D band (D for disorder), appearing at ~1345 cm^{-1}. The evolution of disorder is usually quantified using the well-known Tuinstra-Koenig relation $I_D/I_G = C(\lambda)/L_a$ [3], where I_D/I_G accounts for the intensity ratio between the disorder-induced D band and the Raman-allowed first-order G band (~1585 cm^{-1}). The proportionality constant $C(\lambda)$ depends on the excitation laser wavelength λ. The most commonly used value is $C(\lambda) \sim 4.4$ nm for $\lambda = 488$ nm [3]. Although this relation was developed for measuring the size of crystalline sp^2 clusters (L_a), it has been generally used to quantify the density of defects in sp^2 carbons, including electron [7] and ion [8] bombardment-induced defects in graphene.

In this work the ion bombardment technique is used to gradually induce disorder in graphene and Raman spectroscopy is applied to probe the evolution of disorder. This type of study has been developed previously in graphite [2]. The novelty about graphene is that, in this one-atom thick material, the results are independent of both the penetration depths for the incident light and ions. Our analysis leads us to the formulation of a phenomenological model for the quantification of disorder in graphene. This model is in conceptual agreement with the amorphization trajectory pro-

* *Corresponding author:* Address: Dept. de Física, Universidade Federal de Minas Gerais, Belo Horizonte, MG 30123-970, Brazil. Fax: +55 (31) 34095600.
E-mail address: adojorio@fisica.ufmg.br (A. Jorio).
0008-6223/$ - see front matter
doi:10.1016/j.carbon.2009.12.057

posed by Ferrari and Robertson for graphitic nano-crystallites [5], which describes the evolution of the Raman-based disorder signature I_D/I_G when decreasing the crystallite sizes. On the other hand, our results show that the Tuinstra-Koenig relation [3] should not be applied for a quantitative analysis of ion-induced defects in graphene. Finally, we also extract the Raman relaxation length for the disorder-induced Raman scattering process in graphene. A value that is one order of magnitude lower than what has been published in the literature [9,10] was found.

2. Experiment

Scanning tunneling microscopy (STM) measurements can provide an accurate measure of the defect density. However, direct measure on graphene would require metallization of the sample, which is expected to substantially change its pristine properties by changing the effective Coulomb interactions [11]. For this reason, we adopted a highly oriented pyrolytic graphite (HOPG)-based calibration procedure, as described below.

Initially, consecutive Ar^+ ion bombardment, STM and Raman spectroscopy experiments were performed on bulk HOPG (ZYB grade, $20 \times 20 \times 2$ mm, NT-MDT company). These measurements will be used to calibrate the bombardment procedure that is further applied in this work to the graphene samples. STM imaging (with etched tungsten tips) and ion bombardment experiments (with a partial argon pressure lower than 2×10^{-5} mbar) were carried out in an OMICRON VT-STM ultra-high vacuum system (base pressure 5.0×10^{-11} mbar) equipped with an ISE 5 Ion Source. The ion beam incidence angle was 45° with respect to the normal direction of sample's surface. Low energy ions (90 eV) were used to produce the structural defects. These low energy ions have been experimentally confirmed to barely exceed the threshold value for the displacement of surface C atoms, thereby avoiding cascade effects [12,13]. The bombardment ion doses span the typical values applied for ion implantation studies [2]. We start with 10^{11} Ar^+ impacts per cm^2, which corresponds to one defect per 4×10^4 C atoms, and we go up to 10^{15} Ar^+/cm^2, the limit for full disorder in graphene.

Fig. 1a shows an STM image of the hexagonal honeycomb lattice of the bulk HOPG top layer, prior to the bombardment procedure. Figs. 1b and c show that, up to 10^{12} Ar^+/cm^2, the ion bombardment-induced defects are isolated from each other. Each defect causes a rather large disordered area in the STM images (~1 nm radius, see the inset to Fig. 1b). Near the 10^{13} Ar^+/cm^2 dose (Fig. 1d), the disordered areas start to coalesce. Then the surface exhibits a mixture of ordered and disordered regions (see inset to Fig. 1d). At the 10^{14} Ar^+/cm^2 dose (Fig. 1e) and above, the hexagonal crystalline pattern can no longer be observed by probing the local density of electronic states by STM. Analysis of the STM images at each ion dose gives the defect density σ (or the corresponding ion dose) by the direct counting of defects. From σ we can extract the average distance between defects, $L_D = \frac{1}{\sqrt{\sigma}}$. For the highest ion doses, when the defects start to coalesce, we consider the defect density increases linearly with bombardment time.

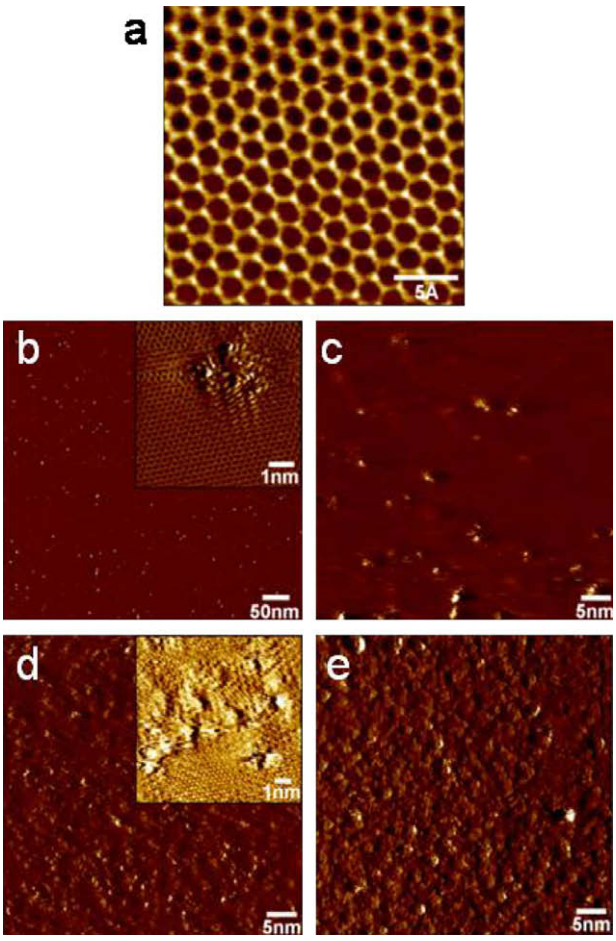

Fig. 1 – STM images of the surface of a bulk HOPG sample subjected to 90 eV Ar^+ ion bombardment. From (a–e) the panels display results at zero, 10^{11}, 10^{12}, 10^{13} and 10^{14} Ar^+/cm^2 ion doses. Insets to (b) and (d) show the detailed atomic structure of the defective areas at their respective ion doses.

For each ion bombardment dose, the bulk HOPG specimen was cleaved in air, immediately inserted into the ultra high vacuum chamber and further transferred to the Raman spectrometer. The micro-Raman scattering measurements were performed with a Horiba Jobin-Ivon T 6400 triple-monochromator equipped with a N_2 cooled charge coupled device (CCD) detector. We apply the backscattering configuration, using a 100× objective (~1 μm^2 beam spot at the sample). The excitation laser energy was 2.41 eV (514.5 nm). Low power (0.25 mW at the microscope objective) was used to avoid heat-induced sample damage or graphitization. To fully calibrate the bombardment procedure that is further applied to the graphene samples, ion bombardment and consecutive Raman measurements on bulk HOPG were performed three times, for up to eight different ion doses between 10^{11} and 10^{15} Ar^+/cm^2. The Raman response was measured at up to 7 locations within the bulk HOPG specimen for each ion dose. Fig. 2 shows the evolution of the bulk HOPG Raman spectra, where we chose only one representative spectrum of each ion bombardment dose displayed in Fig. 1. The spectra in Fig. 2 will be used in this work for calibration of the graphene sample measurements, as discussed in Section 3.1.

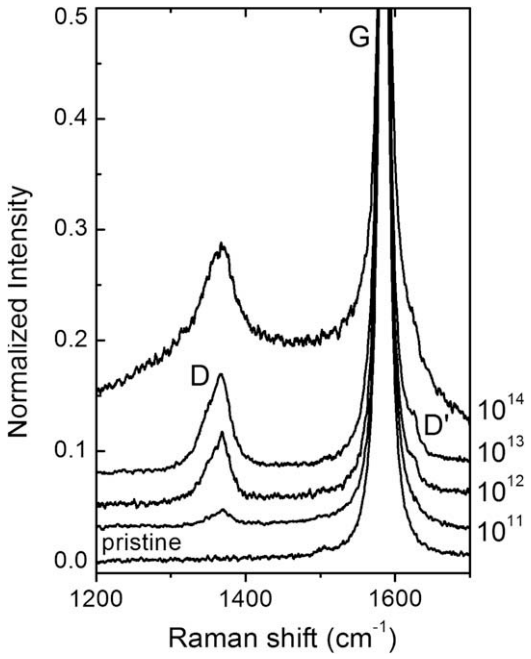

Fig. 2 – Evolution of the first-order Raman spectra of the same bulk HOPG sample displayed in Fig. 1, measured after each bombardment and STM imaging procedures. We use a λ = 514 nm laser. The ion doses are displayed next to the respective spectrum in units of Ar$^+$/cm^2. Each spectrum is normalized to its respective G band and the results for each sample are displaced vertically for clarity.

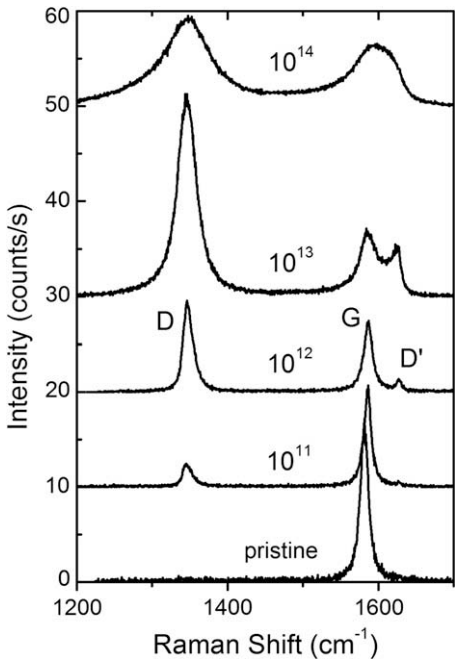

Fig. 3 – Evolution of the first-order Raman spectra of a monolayer graphene sample deposited on an SiO_2 substrate, subjected to the same ion bombardment conditions as are shown in Figs. 1 and 2, using a λ = 514 nm laser. The ion doses are indicated next to the respective spectrum in units of Ar$^+$/cm^2. The spectra in this figure are also displaced vertically for clarity. A second disorder-induced peak around ~1620 cm^{-1} (named the D′ band) also appears, but we do not focus on this feature here.

Finally, three different graphene samples (all single-layer, tens of μm in size) were prepared from mechanical exfoliation of the same bulk HOPG specimen, and deposited onto a Si substrate with a 300 nm layer of SiO_2, following a nowadays broadly used procedure [14]. No further cleaning or processing was applied to the graphene samples to avoid changing its pristine properties. Optical microscopy was used to map the graphene sample location on the Si/SiO_2 substrate [14]. The single-layer graphene samples were identified by both Raman spectroscopy [15] and atomic force microscopy (AFM instrument from JPK company, in the tapping mode under ambient conditions). In one of the samples, a small HOPG flake (~50-layers in thickness, as inferred from its AFM height) was found nearby. The correlation between the ion bombardment-induced effects on the Raman spectra of bulk HOPG (Fig. 2) and of this ~50-layer HOPG confirms that the ion bombardment calibration procedure developed for HOPG applies to the single-layer graphene samples (more details are found in Section 3.1). For the graphene experiments, the Si/SiO_2 substrate Raman peak in the 950–1000 cm^{-1} range was measured and used to check the Raman intensity calibration.

3. Results and discussion

3.1. *Raman spectroscopy results on ion bombarded graphene*

Fig. 3 shows the Raman spectra of graphene subjected to the same ion dose bombardments shown in Figs. 1 and 2. From the pristine sample to the lowest bombardment dose in Fig. 3 (10^{11} Ar$^+$/cm^2), the D band scattering process is activated, leading to the observation of a very small intensity D peak, as compared to the G peak. By increasing the bombardment dose, the intensity of the disorder peak increases. Above 10^{13} Ar$^+$/cm^2 the Raman peaks start to broaden significantly, with no change in peak frequencies. This description is similar to what has been observed for bulk HOPG (see Fig. 2), although some details are different. Firstly, for HOPG a larger G band is always observed due to the contribution from the undisturbed under-layers. Secondly, for graphene, above 10^{15} Ar$^+$/cm^2 the spectra show a decreased intensity, indicating full amorphization or partial sputtering of the graphene layer. For HOPG, above 10^{15} Ar$^+$/cm^2 I_D/I_G saturates and no further change is observed in the Raman spectra because of the large number of layers to be amorphized and/or sputtered. Thirdly and even more important, the quantitative development of the I_D/I_G ratio for graphene and graphite are very different, as shown below.

The I_D/I_G values are here obtained by considering the peak intensity at the fixed D- (1345 cm^{-1}) and G-band (1585 cm^{-1}) frequencies. To quantify the development of disorder in graphene, we plot the I_D/I_G data as a function of the average distance between defects L_D, as shown in Fig. 4. The inset to Fig. 4 stands for the HOPG-based ion dose calibration. The I_D/I_G evolution for the ~50-layer HOPG (bullets) is compared with the I_D/I_G observed in the bulk HOPG (diamonds). The dif-

ferences in absolute values depend on the light penetration depth and on the number of layers. For this reason, the bulk HOPG data in the inset to Fig. 4 had to be scaled by ×3.5 to fit the 50-layers HOPG values. However, the I_D/I_G values increase and saturate at the same ion doses, showing that the ion doses are the same and the calibration procedure was accurate. Now moving to the main panel of Fig. 4, the I_D/I_G has a non-monotonic dependence on L_D, increasing with increasing L_D up to $L_D \sim 4$ nm, and then decreasing for $L_D > 4$ nm. Such behavior suggests the existence of two disorder-induced competing mechanisms contributing to the Raman D band. These competing mechanisms are the basis for our phenomenological model for the L_D dependence of I_D/I_G that is developed in the next section.

3.2. *Modeling the I_D/I_G vs. L_D dependence*

We model the results in Fig. 4 considering that a single impact of an ion on the graphene sheet causes modifications on two length scales, here denoted by r_A and r_S (with $r_A > r_S$), which are the radii of two circular areas measured from the impact point (see Fig. 5). Within the shorter radius r_S, structural disorder from the impact occurs, as shown in the inset to Fig. 1b. We call this the *structurally-disordered* or S-region. For distances larger than r_S but shorter than r_A, the lattice structure is preserved, but the proximity to a defect causes a mixing of Bloch states near the K and K' valleys of the graphene Brillouin zone, thus causing a breaking of selection rules, and leading to an enhancement of the D band. We call this the *activated* or A-region. In qualitative terms, an electron–hole excitation will only be able to "see" the structural defect

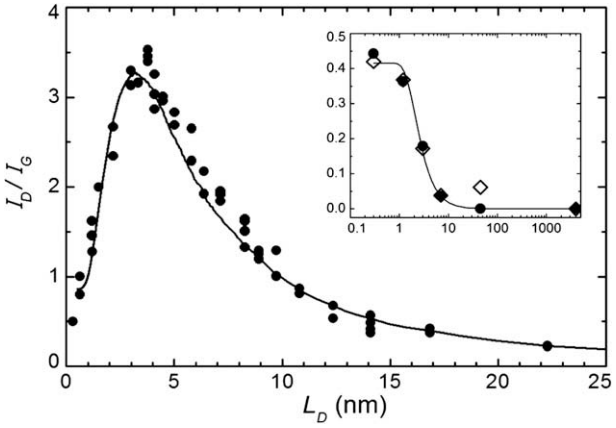

Fig. 4 – The I_D/I_G data points from three different mono-layer graphene samples as a function of the average distance L_D between defects, induced by the ion bombardment procedure. We use intensity ratio rather than integrated area ratio because, below $L_D \sim 5$ nm, the G and D′ peaks overlap. The solid line is a modeling of our data with Eq. (1). The inset shows the I_D/I_G vs. L_D on a log scale for two graphite samples: (i) a ~50-layer graphene sample found near one of the three mono-layer graphene samples (bullets); (ii) the bulk HOPG sample used for calibration (diamonds). The bulk HOPG values are here scaled by (I_D/I_G) × 3.5.

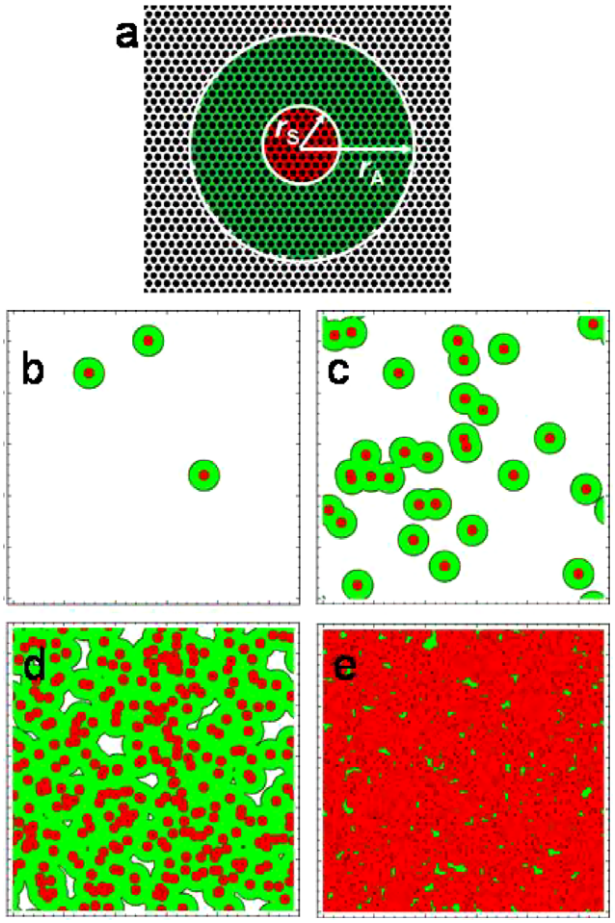

Fig. 5 – (a) Definition of the "*activated*" A-region (green) and "*structurally-disordered*" S-region (red). The radii are measured from the impact point which is chosen randomly in our simulation. (b–e) shows 55 × 55 nm portions of the graphene simulation cell, with snapshots of the structural evolution of the graphene sheet for different defect concentrations: (b) 10^{11} Ar^+/cm^2; (c) 10^{12} Ar^+/cm^2; (d) 10^{13} Ar^+/cm^2; (e) 10^{14} Ar^+/cm^2, like in Fig. 1.

if it is created sufficiently close to it and if the excited electron (or hole) lives long enough for the defective region to be probed by Raman spectroscopy. If the Raman scattering process occurs at distances larger than $\ell = r_A - r_S$ from the defective region, the wavevector $\mathbf{k}$ is a good quantum number for analyzing the scattering selection rules and those regions will only contribute to the G band. Our phenomenological model for the I_D/I_G ratio is given by:

$$\frac{I_D}{I_G}(L_D) = C_A f_A(L_D) + C_S f_S(L_D), \quad (1)$$

where f_A and f_S are simply the fractions of the A and S areas in the sheet, respectively, with respect to the total area. The A-regions will contribute most strongly to the D band, while the S-regions will make less contribution to the D band due to breakdown of the lattice structure itself.

We now describe the stochastic simulations (see Fig. 5b–e) used to implement our phenomenological model for the I_D/I_G ratio. The structurally-disordered (S) region is shown in red in Fig. 5a and the activated (A) region is shown in green in

Fig. 5a. We simulate the structural evolution of a graphene sheet under ion bombardment by randomly choosing a sequence of impact positions on a ($100 \times 100\ nm^2$) sheet. We define the following set of rules for each event: (1) Pristine regions (white area in Fig. 5b–e) may turn into *S* (red) or *A* (green), depending on the proximity to the impact point; (2) Similarly, *A*-regions may turn into *S* (red); (3) *S*-regions always remain *S*. Then, the initially pristine sheet evolves, as the number of impacts increase, to be mostly activated, leading to an increase of the D band. In sequence, the mostly structurally-disordered regions become increasingly widespread, leading to a decrease of the D band. Snapshots of this evolution are shown in Fig. 5b–e for the same concentrations as Fig. 1b–e. Our stochastic simulations of the bombardment process, with the impact points for the ions chosen at random, combined with Eq. (1) with parameters $C_A = 4.56$, $C_S = 0.86$, $r_A = 3$ nm and $r_S = 1$ nm, gives the full line curve in Fig. 4, which is in excellent agreement with the experimental results in this figure.

3.3. Discussion

The non-monotonic behavior can be understood by considering that, for low defect density (large L_D), the total area contributing to scattering is proportional to the number of defects, giving rise to a $I_D/I_G = (102 \pm 2)/L_D^2$ dependence that works well for $L_D > 2r_A$. This result is based on geometry. If we consider an edge (one-dimensional) defect, rather than a point defect, as it is appropriate for crystallites of nanometer-scale sizes L_a [3,5], our model gives an $I_D/I_G \propto 1/L_a$ dependence, in agreement with the Tuinstra-Koenig relation [3].

Upon increasing the defect density, the activated regions start to overlap and these regions eventually saturate. The D band intensity then reaches a maximum. Further increase in the defect density decreases the D band intensity because the graphene sheet starts to be dominated by the structurally-disordered areas.

The length scale $r_S = 1$ nm, which defines the structurally-disordered area, is in agreement with the size of the disordered structures seen in the STM images (see inset to Fig. 1b). This parameter should not be universal, but it is typical to our bombardment process. The Raman relaxation length for the resonant Raman scattering in graphene for a laser energy of 2.41 eV is found to be $\ell = r_A - r_S = 2$ nm. This ℓ value is one order of magnitude smaller as compared with reported values [9,10], and in better agreement with the $\ell = 4$ nm value estimated in [16,17]. The C_A parameter in Eq. (1) is a measure of the maximum possible value of the I_D/I_G ratio in graphene. C_A would occur in a hypothetical situation in which $K - K'$ wavevector mixing would be allowed everywhere, but no damage would be made to the hexagonal network of carbon atoms. C_A should then be defined by the electron–phonon matrix elements, and the value $C_A = 4.56$ is in rough agreement with the ratio between electron–phonon coupling for the optical phonons evaluated between the Γ and *K* points [18]. The C_S parameter is the value of the I_D/I_G ratio in the highly disordered limit, which has not yet been addressed theoretically.

Finally, Fig. 6 compares our results with the amorphization trajectory proposed by Ferrari and Robertson [5] (see details in the caption to Fig. 6). In general, our experimental data validate the proposed trends. However, our model is quantitatively more accurate for describing the evolution of I_D/I_G with L_D for ion-induced defects in graphene.

3.4. Rate equations for practical usage

For practical means, we can obtain an analytic expression for I_D/I_G as a function of $L_D = \sigma^{-1/2}$ by solving the following rate equations for the evolution of the *S*- and *A*-regions:

$$\frac{dS_S}{dN} = \pi r_S^2\left(\frac{S_T - S_S}{S_T}\right) \tag{2}$$

$$\frac{dS_A}{dN} = \pi(r_A^2 - r_S^2)\left(\frac{S_T - S_S - S_A}{S_T}\right) \tag{3}$$

where S_S, S_A and S_T denote the structurally disordered, activated and total areas of the sheet, respectively, and *N* is the number of Ar^+ impacts. These equations are consistent with the rules for the stochastic simulations described in Section 3.2. In terms of the area fractions $f_A = S_A/S_T$, $f_S = S_S/S_T$ and $\sigma = N/S_T$, these equations become

$$\frac{df_S}{d\sigma} = \pi r_S^2(1 - f_S) \tag{4}$$

$$\frac{df_A}{d\sigma} = \pi(r_A^2 - r_S^2)(1 - f_S - f_A) \tag{5}$$

These simple rate equations can be solved analytically. With the initial conditions $f_S = 0$ and $f_A = 0$ for $\sigma = 0$, and expressing the results in terms $L_D = \sigma^{-1/2}$, the solutions are:

$$f_S(L_D) = (1 - e^{-\pi r_S^2/L_D 2}) \tag{6}$$

$$f_A(L_D) = \frac{r_A^2 - r_S^2}{r_A^2 - 2r_S^2}(e^{-\pi r_S^2/L_D 2} - e^{-\pi(r_A^2 - r_S^2)/L_D 2}). \tag{7}$$

Finally, the entire regime ($0 \to L_D \to \infty$) can be fitted using:

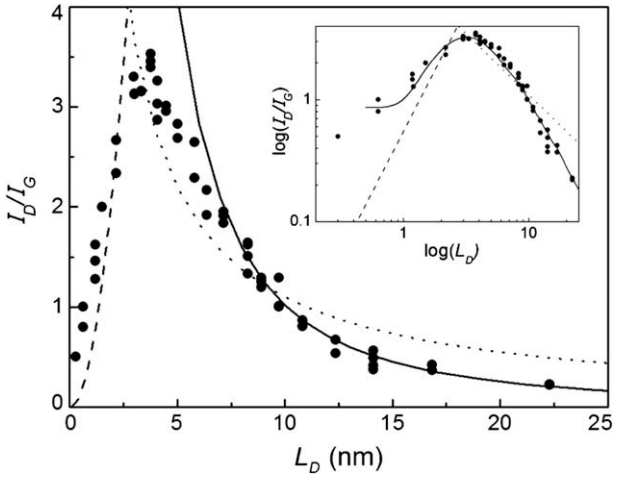

Fig. 6 – Comparison of the I_D/I_G data points from Fig. 4 with the amorphization trajectory proposed by Ferrari and Robertson [5]. The dashed, dotted and solid lines are given by $I_D/I_G = 0.0055L_D^2$ (from Ref. [5]), $I_D/I_G = 11/L_D$ (from Ref. [3] with a 2.5 times larger proportionality constant to fit the data) and $I_D/I_G = 102/L_D^2$ (this work), respectively. The inset shows the same plot in a log–log scale, but replacing the $I_D/I_G = 102/L_D^2$ relation by our full model, as given by Eq. (1) (solid line).

$$I_D/I_G = C_A \frac{r_A^2 - r_S^2}{r_A^2 - 2r_S^2}[\exp(-\pi r_S^2/L_D^2) - \exp(-\pi(r_A^2 - r_S^2)/L_D^2)] + C_S[1 - \exp(-\pi r_S^2/L_D^2)] \quad (8)$$

A fit of Eq. (5) to our data in Fig. 4 gives $C_A = (4.2 \pm 0.1)$, $C_S = (0.87 \pm 0.05)$, $r_A = (3.00 \pm 0.03)$ nm and $r_S = (1.00 \pm 0.04)$ nm, also in excellent agreement with experiment and consistent with the parameters obtained within our computational modeling.

5. Summary

We measured the effect of disorder in the Raman spectra of graphene subjected to low energy Ar^+ ion bombardment, sweeping across the two length scales that characterize ion-induced lattice disorder (r_S) and Raman scattering electron-relaxation ($\ell = r_A - r_S$). Our model provides a method to quantify the density of defects σ or, equivalently, the average distance between defects $L_D = \frac{1}{\sqrt{\sigma}}$ in graphene. Before the defects start to coalesce ($L_D > 6$ nm in our case), the expected behavior occurs, i.e. $I_D/I_G = A/L_D^2 \propto \sigma$, where $A = (102 \pm 2)$ nm^2 was found. When the defects start to coalesce there is a competition between two disorder mechanisms, and Eq. (8) can be used for quantitative analysis to determine the relative importance of each mechanism. Our results allowed us to extract the Raman relaxation length ℓ for the disorder-induced Raman scattering process in graphene. We found the value $\ell = 2$ nm, which is the value valid for our excitation laser wavelength $\lambda = 514$ nm, but this value is expected to depend on λ [6,17]. The I_D/I_G results on HOPG are different from those on mono-layer graphene, showing an increase and saturation of I_D/I_G with decreasing L_D. It would be interesting to extend this work to bilayer, trilayer graphene samples. At some point, the evolution has to converge to the HOPG result, thus giving important information about the penetration depth of ions and light.

Finally, our phenomenological model can also be used to obtain the Tuinstra-Koenig relation [3] $I_D/I_G \propto 1/L_a$, by considering the crystallite border as an extended (one-dimensional) defect structure, and by changing the crystallite size L_a. To use our results to obtain the constant C for the Tuinstra-Koenig relation, one has to know r_S. Since r_S may change from sample to sample, it is expected that different experiments would give different proportionality constants for $I_D/I_G = C/L_a$, as already stated by Cuesta et al. [19]. Our results may be useful to study the amorphous structure of the crystallite borders.

Acknowledgement

We acknowledge L.G. Cançado and H. Niehus for helpful discussions and financial support from the Brazilian Agencies CNPq, FINEP and FAPERJ and from the American Agency AFOSR/SOARD (award #FA9550-08-1-0236).

REFERENCES

[1] Castron Neto AH, Guinea F, Perer NM, Geim AK. The electronic properties of graphene. Rev Mod Phys 2009;81:109.
[2] Dresselhaus MS, Kalish R. Ion implantation in diamond, graphite and related materials. Berlin: Springer-Verlag; 1992. and references contained therein.
[3] Tuinstra F, Koenig JL. Raman spectrum of graphite. J Chem Phys 1970;53(3):1126–30.
[4] Dillon RO, Woollam JA, Katkanant V. Use of Raman scattering to investigate disorder and crystallite formation in as-deposited and annealed carbon films. Phys Rev B 1984;29(6):3482–9.
[5] Ferrari AC, Robertson J. Interpretation of Raman spectra of disordered and amorphous carbon. Phys Rev B 2000;61(20):14095–107.
[6] Cançado LG, Takay K, Enoki T, Endo M, Kim YA, Mizusaki H, et al. General equation for the determination of the crystallite size L_a of nanographite by Raman spectroscopy. Appl Phys Lett 2006;88:163106.
[7] Teweldebrhan D, Baladin AA. Modification of graphene properties due to electron-beam irradiation. Appl Phys Lett 2009;94:013101.
[8] Chen JH, Cullen WG, Jang C, Fuhrer MS, Williams ED. Defect scattering in graphene. Phys Rev Lett 2009;102:236805.
[9] Cançado LG, Beams R, Novotny L. Optical measurement of the phase-breaking length in graphene. arXiv: 0802.3709.
[10] Gupta AK, Russin TJ, Gutiérrez HR. Eklund PC probing graphene edges via Raman scattering. ACSNano 2009;3(1):45–52.
[11] Lee J, Eggert S, Kim H, Kahng S-J, Shinohara H, Kuk Y. Real space imaging of one-dimensional standing waves: direct evidence for a Luttinger liquid. Phys Rev Lett 2004;93:166403-1–4.
[12] Hahn JR, Kang H. Vacancy and interstitial defects at graphite surfaces: scanning tunneling microscopy study of the structure, electronic property and yield for ion-induced defect creation. Phys Rev B 1999;60(8):6007–17.
[13] Marton D, Bu H, Boyd KJ, Todorov SS, Al-Bayati AH, Rabalais JW. On the defect structure due to low energy ion bombardment of graphite. Surf Sci Lett 2005;326:L489–93.
[14] Geim AK, Novoselov KS. The rise of graphene. Nat Mater 2007;6:183–91.
[15] Ferrari AC, Meyer JC, Scardaci V, Casiraghi C, Lazzeri M, Mauri F, et al. Raman spectrum of graphene and graphene layers. Phys Rev Lett 2006;97:187401.
[16] Casiraghi C, Hartschuh A, Qian H, Pisanec S, Georgi C, Fasoli A, et al. Raman spectroscopy of graphene edges. Nano Lett 2009;9:1433.
[17] Basko DM. Boundary problems for Dirac electrons and edge-assisted Raman scattering in graphene. Phys Rev B 2009;79:205428.
[18] Lazzeri M, Attaccalite C, Wirtz L, Mauri F. Impact of the electron-electron correlation on phonon dispersion: failure of LDA and GGA DFT functionals in graphene and graphite. Phys Rev B 2008;78:081406R.
[19] Cuesta A, Dhamelincourt P, Laureyns J, Martínez-Alonso A, Tascón JMD. Comparative performance of X-ray diffraction and Raman microprobe techniques for the study of carbon materials. J Mater Chem 1998;8:2875–9.